

# The Johns Hopkins Turbulence Databases (*JHTDB*)

## HOMOGENEOUS BUOYANCY DRIVEN TURBULENCE DATA SET

*Data provenance:* D. Livescu<sup>1</sup>

*Database Ingest and Web Services:* C. Canada<sup>1</sup>, K. Kalin<sup>2</sup>, R. Burns<sup>2</sup> & IDIES staff

*Visualization:* J. Pulido<sup>1,3</sup>

<sup>1</sup>Los Alamos National Laboratory, Los Alamos, NM 87544

<sup>2</sup>Johns Hopkins University, Baltimore, MD 21218

<sup>3</sup>University of California, Davis, CA 95616

The data is from a direct numerical simulation (DNS) of homogeneous buoyancy driven turbulence on a  $1024^3$  periodic grid. The equations solved are the miscible two-fluid incompressible Navier-Stokes equations, which are obtained from the fully compressible Navier-Stokes equations with two species with different molar masses in the limit  $c \rightarrow \infty$  ( $c$  is the speed of sound) such that the individual densities of the two fluids remain constant [1, 2, 3]:

$$\frac{\partial}{\partial t}\rho + (\rho u_j)_{,j} = 0 \quad (1)$$

$$\frac{\partial}{\partial t}(\rho u_i) + (\rho u_i u_j)_{,j} = -p_{,i} + \tau_{ij,j} + \frac{1}{Fr^2}\rho g_i \quad (2)$$

$$u_{j,j} = -\frac{1}{Re_0 Sc}(\ln\rho)_{,jj}, \quad (3)$$

where  $\rho$  is the density of the mixture (defined according to  $\rho = (Y_1/\rho_1 + Y_2/\rho_2)^{-1}$  with  $Y_1 + Y_2 = 1$  being the mixture fractions and  $\rho_1$  and  $\rho_2$  the fluids' individual densities [1]),  $u_i$  is the mixture's velocity vector field and  $p$  the pressure. The viscous stress is Newtonian with

$$\tau_{ij} = \frac{\rho}{Re_0}[u_{i,j} + u_{j,i} - \frac{2}{3}u_{k,k}\delta_{ij}] \quad (4)$$

Note that Eqs. (1)-(2) are the usual continuity and momentum transport equations for compressible flows. Equations (1)-(3) describe the mixing, at any density ratio, between incompressible materials or compressible materials in low speed, low acceleration flows, when the fluids participating in the mixing maintain quasi-constant microscopic densities. If the densities of the two fluids are commensurate, then the mixture density is close to its average value and Eqs. (1)-(3) lead to the Boussinesq approximation (see Ref. [1] for the derivation). An example of DNS of such flow in the Boussinesq limit can be found in Ref. [4]. Note that the divergence of velocity is not zero for the non-Boussinesq case, as the specific volume changes during mixing.

The nondimensional parameters are the computational Reynolds number,  $Re_0$ , Schmidt number,  $Sc$ , and Froude number,  $Fr$ .  $g_i$  are the components of the unit vector in the direction of gravity,  $\vec{g} = (1, 0, 0)$ , and the kinematic viscosity,  $\nu_0 = \mu/\rho$ , and mass diffusion coefficient,  $\mathcal{D}$ , are assumed constant, such that  $Sc$  is uniform throughout the flow. The independent variables are the time  $t$  and space variables,  $x_i$ . Equations (1)-(3) have periodic boundary conditions and the homogeneity of the fluctuating quantities is ensured by imposing mean zero velocity and constant mean pressure gradient [1]. These conditions are similar to those encountered in the interior of the Rayleigh-Taylor mixing layer during the turbulent stage [5]. Eqs. 1-3 are solved using a pseudo-spectral approach,

with the skew-symmetric form of the advection terms to minimize aliasing errors, and the third order predictor-corrector Adams-Bashforth-Moulton scheme coupled with a pressure projection method for time advancement.

The simulation was performed with the variable-density version of the petascale CFDNS code [6]. The two fluids are initialized as random blobs, consistent with the homogeneity assumption. The flow starts from rest, with only a small amount of dilatational velocity necessary to satisfy condition 3, and turbulence is generated as the two fluids start moving in opposite directions due to differential buoyancy forces. However, as the fluids become molecularly mixed, the buoyancy forces decrease and at some point the turbulence starts decaying. The database covers both the buoyancy driven increase in turbulence intensity as well as the buoyancy mediated turbulence decay. All averages are calculated as volume averages. Below, fluctuations about the Reynolds averages are denoted by primes, while fluctuations about Favre (density weighted) averages are denoted by double primes.

### Simulation parameters

Domain:  $2\pi \times 2\pi \times 2\pi$  (i.e. range of  $x_1$ ,  $x_2$ , and  $x_3$  is  $[0, 2\pi]$ )

Grid:  $1024^3$

Computational Reynolds number: 12,500 (inverse of the non-dimensional kinematic viscosity,  $1/\nu$ )

Schmidt number: 1.0

Froude number: 1.0

Density of pure light fluid: 1.0

Density of pure heavy fluid:  $1.0/0.95 \approx 1.105$

Atwood number: 0.05

Mean density:  $\approx 1.053$

Initial density integral lengthscale:  $\approx 1.382$

Initial density variance:  $\approx 0.002681$

Minimum DNS time step:  $8 \times 10^{-4}$

Maximum DNS time step:  $2 \times 10^{-3}$

Database time step:  $4 \times 10^{-2}$

Time stored: from  $t = 0$  to  $t = 40.56$  (1015 datafiles)

### Flow statistics

Maximum turbulent Reynolds number:  $Re_t = \frac{\tilde{k}^2}{\nu\epsilon} \approx 17,765$

Time at maximum  $Re_t$ : 6.56

Maximum Favre kinetic energy:  $\tilde{k} = \frac{\langle \rho u_i'' u_i'' \rangle}{2\langle \rho \rangle} = 0.03973$  (at time 11.4).

$\tilde{k}$  at maximum  $Re_t$ : 0.02388

Maximum eddy turnover time:  $\tau = \frac{\tilde{k}}{\epsilon} = 77.63$  (at time 4.2).

$\tau$  at maximum  $Re_t$ : 59.52 and at maximum  $\tilde{k}$ : 12.82.

Maximum turbulent kinetic energy dissipation:  $\epsilon = 0.005332$  (at time 14.56)

$\epsilon$  at maximum  $Re_t$ : 0.0004012 and at maximum  $\tilde{k}$ : 0.003098.

Several quantities from the simulation are shown in the figures below. Figures 1-5 show the time evolutions of turbulent Reynolds number, Favre turbulent kinetic energy, Reynolds stresses in the direction of gravity,  $R_{vv} = \langle \rho u_1'' u_1'' \rangle$ , and perpendicular to gravity,  $R_{hh} = (\langle \rho u_2'' u_2'' \rangle + \langle \rho u_3'' u_3'' \rangle)/2$ , and vertical mass flux,  $a_v = \langle \rho u_1' \rangle / \langle \rho \rangle$ , eddy turnover time, kinetic energy dissipation, density variance and density-specific volume correlation, respectively. Figure 6 shows the density PDF at different times. Finally, figure 7 shows the 3-D power spectra of density,  $E_{\rho\rho}$ , vertical and horizontal velocities,  $E_{vv} = E_{11}$  and  $E_{hh} = (E_{22} + E_{33})/2$ , and density vertical

velocity co-spectrum,  $E_{v\rho}$ , at  $t = 6.56$  and  $t = 11.4$ .

**Acknowledgments:** Los Alamos National Laboratory is operated by the Los Alamos National Security, LLC for the U.S. Department of Energy NNSA under contract no. DE-AC52-06NA25396. Computational resources for the simulation described here were provided by LANL Institutional Computing (IC) Program.

## References

- [1] D. Livescu and J. R. Ristorcelli. Buoyancy-driven variable-density turbulence. *J. Fluid Mech.*, 591:43–71, 2007.
- [2] D. Livescu and J. R. Ristorcelli. Variable-density mixing in buoyancy-driven turbulence. *J. Fluid Mech.*, 605:145–180, 2008.
- [3] D. Livescu. Numerical simulations of two-fluid turbulent mixing at large density ratios and applications to the Rayleigh-Taylor instability. *Phil. Trans. R. Soc. A*, 371:20120185, 2013.
- [4] G. K. Batchelor, V. M. Canuto, and J. R. Chasnov. Homogeneous buoyancy-generated turbulence. *J. Fluid Mech.*, 235:349–378, 1992.
- [5] D. Livescu, J. R. Ristorcelli, R. A. Gore, S. H. Dean, W. H. Cabot, and A. W. Cook. High-Reynolds number Rayleigh-Taylor turbulence. *J. Turbul.*, 10:N13, 2009.
- [6] D. Livescu, J. Mohd-Yusof, M. R. Petersen, and J. W. Grove. CFDNS: A computer code for direct numerical simulation of turbulent flows. Technical report, Los Alamos National Laboratory, 2009. LA-CC-09-100.

\* *Note:* The velocity divergence condition (Eq. 3) in the simulation is enforced based on the spectral representation of the derivatives. The JHTDB analysis tools for gradients are based on finite differencing of various orders. Therefore, when evaluating the divergence using these spatially more localized derivative operators, a non-negligible error in the divergence is obtained, as expected.

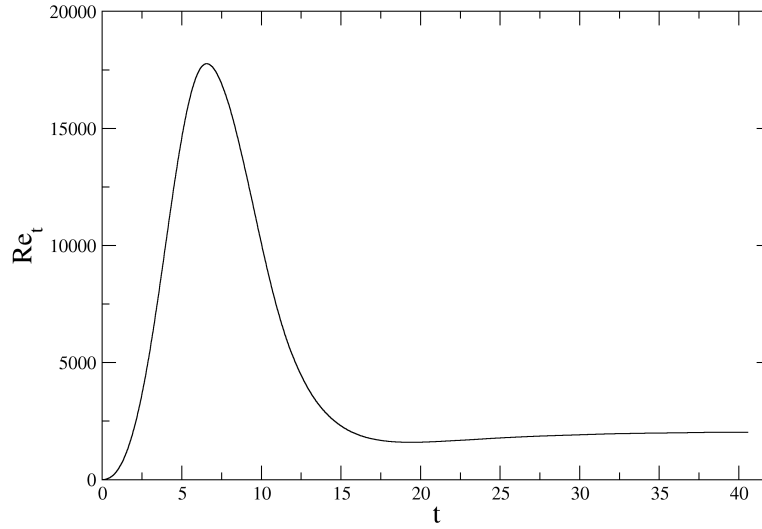


Figure 1: Evolution of turbulent Reynolds number.

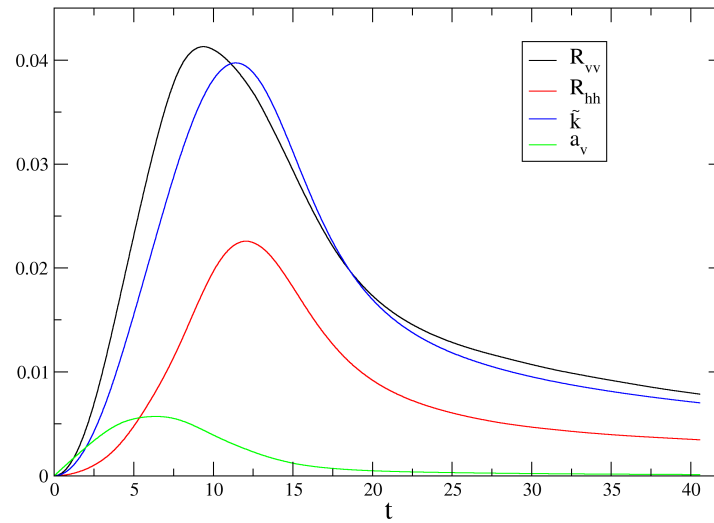


Figure 2: Evolution of Favre turbulent kinetic energy, vertical and horizontal Favre Reynolds stresses,  $R_{vv} = \langle \rho u_1'' u_1'' \rangle$  and  $R_{hh} = (\langle \rho u_2'' u_2'' \rangle + \langle \rho u_3'' u_3'' \rangle)/2$ , and vertical mass flux,  $a_v = \langle \rho u_1' \rangle / \langle \rho \rangle$ .

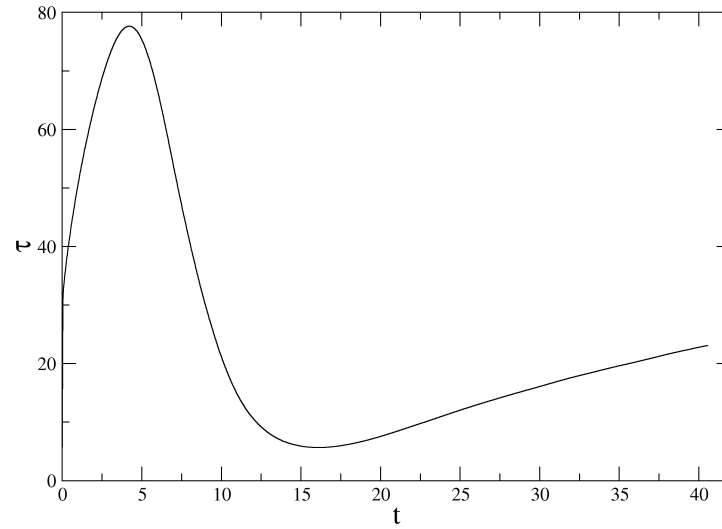


Figure 3: Evolution of eddy turnover time.

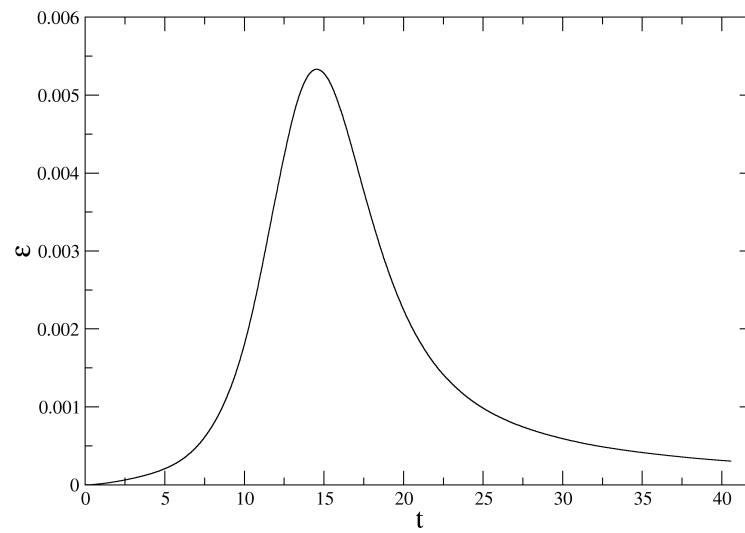


Figure 4: Evolution of Favre turbulent kinetic energy dissipation.

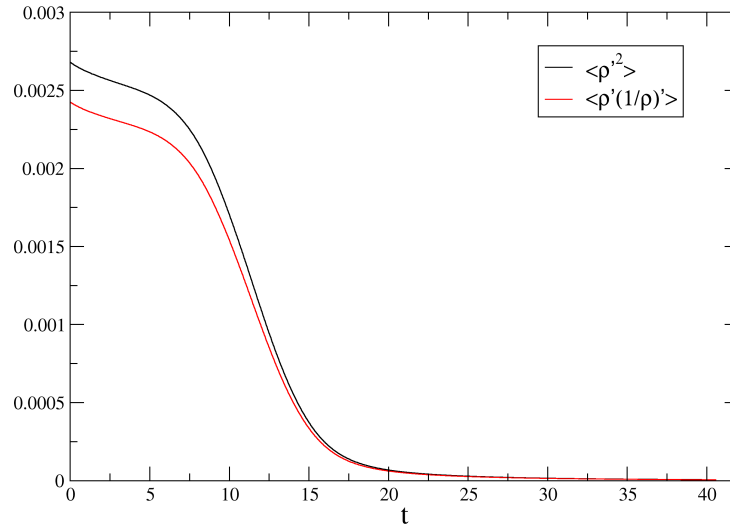


Figure 5: Evolution of density variance and density-specific volume correlation.

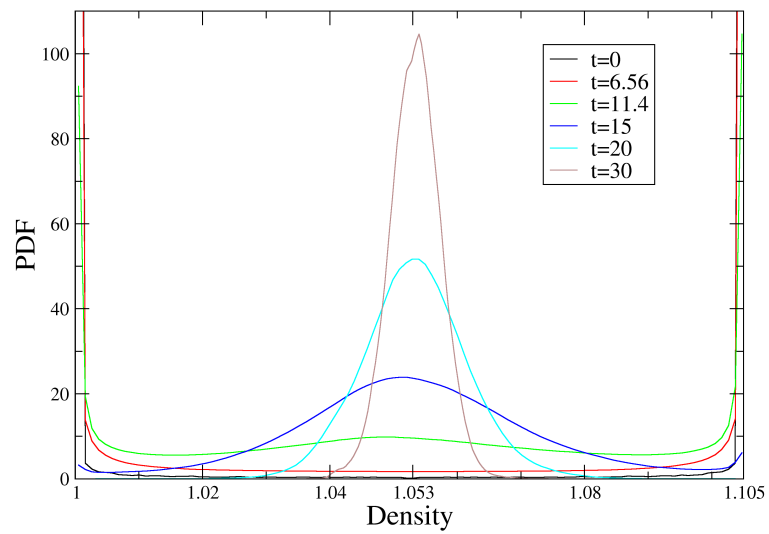


Figure 6: Density PDF at different times.

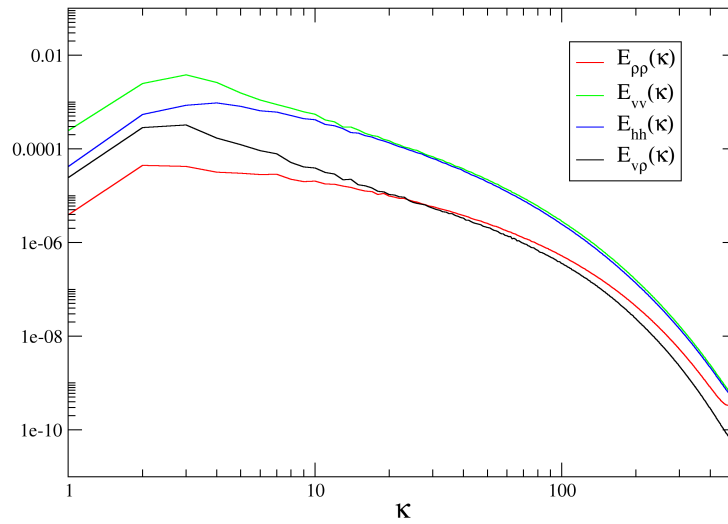
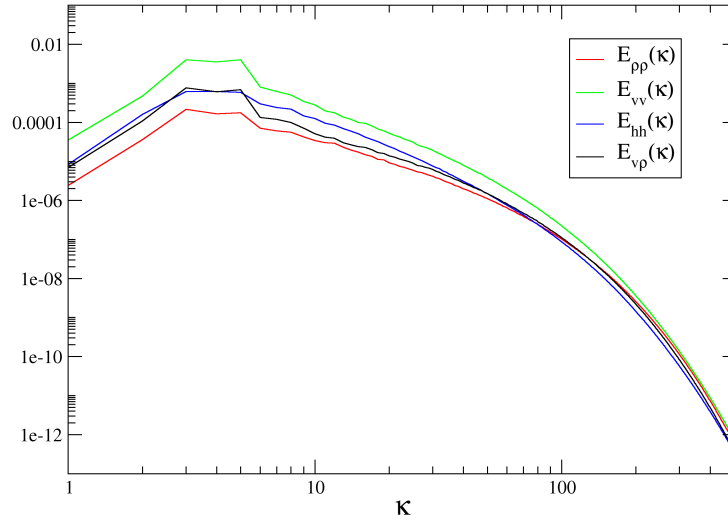


Figure 7: 3-D power spectra of density,  $E_{\rho\rho}$ , vertical and horizontal velocity components,  $E_{vv} = E_{11}$  and  $E_{hh} = (E_{22} + E_{33})/2$ , and density vertical velocity co-spectrum,  $E_{v\rho}$ , at a)  $t=6.56$  (maximum  $Re_t$ ) and b)  $t=11.4$  (maximum  $\tilde{k}$ ).